

Number Density Distribution of Near-Infrared Sources on a Sub-Degree Scale in the Galactic Center: Comparison with the Fe xxv $K\alpha$ Line at 6.7 keV

Kazuki YASUI¹, Shogo NISHIYAMA², Tatsuhito YOSHIKAWA¹, Schun NAGATOMO¹, Hideki UCHIYAMA³, Takeshi Go TSURU⁴, Katsuji KOYAMA^{4, 5}, Motohide TAMURA⁶, Jungmi KWON⁶, Koji SUGITANI⁷, Rainer SCHÖDEL⁸, and Tetsuya NAGATA¹

¹Department of Astronomy, Graduate School of Science, Kyoto University, Kyoto 606-8502

²Miyagi University of Education, Aoba-ku, Sendai 980-0845

³Science Education, Faculty of Education, Shizuoka University, Shizuoka 422-8529

⁴Department of Physics, Graduate School of Science, Kyoto University, Kyoto 606-8502

⁵Department of Earth and Space Science, Graduate School of Science, Osaka University, Osaka 560-0043

⁶Department of Astronomy, Graduate School of Science, The University of Tokyo, Tokyo 113-0033

⁷Graduate School of Natural Sciences, Nagoya City University, Nagoya 467-8501

⁸Instituto de Astrofísica de Andalucía (CSIC), Glorieta de la Astronomía s/n, 18008, Granada, Spain

*E-mail: yasui@kusastro.kyoto-u.ac.jp, nagata@kusastro.kyoto-u.ac.jp

Received ; Accepted

Abstract

The stellar distribution derived from an H and K_S -band survey of the central region of our Galaxy is compared with the Fe xxv $K\alpha$ (6.7 keV) line intensity observed with the Suzaku satellite. The survey is for the Galactic coordinates $|l| \lesssim 3^\circ.0$ and $|b| \lesssim 1^\circ.0$ (equivalent to

$0.8 \text{ kpc} \times 0.3 \text{ kpc}$ for $R_0 = 8 \text{ kpc}$), and the number-density distribution $N(K_{S,0}; l, b)$ of stars is derived using the extinction-corrected magnitude $K_{S,0} = 10.5$. This is deep enough to probe the old red giant population and in turn to estimate the (l, b) distribution of faint X-ray point sources such as coronally active binaries and cataclysmic variables. In the Galactic plane ($b = 0^\circ$), $N(10.5; l, b)$ increases to the Galactic center as $|l|^{-0.30 \pm 0.03}$ in the range of $-0^\circ.1 \geq l \geq -0^\circ.7$, but this increase is significantly slower than the increase ($|l|^{-0.44 \pm 0.02}$) of the Fe XXV $K\alpha$ line intensity. If normalized with the ratios in the outer region $1^\circ.5 \leq |l| \leq 2^\circ.8$, where faint X-ray point sources are argued to dominate the diffuse Galactic X-ray ridge emission, the excess of the Fe XXV $K\alpha$ line intensity over the stellar number density is at least a factor of two at $|l| = 0^\circ.1$. This indicates that a significant part of the Galactic center diffuse emission arises from a truly diffuse optically-thin thermal plasma, and not from an unresolved collection of faint X-ray point sources related to the old stellar population.

Key words: Galaxy: center — infrared: stars — ISM: lines and bands — X-rays: spectra

1 Introduction

The Galactic center diffuse X-rays (GCDX) were found as a flux peak having strong emission lines around 6.7 keV with a spatial width of $\sim 1^\circ$ (Koyama et al. 1989) in the Galactic ridge X-ray emission (GRXE). The emission was resolved into three lines at 6.4, 6.7, and 7.0 keV arising from neutral, He-like, and H-like iron (Koyama et al. 1996), respectively. The 6.7 keV $K\alpha$ line from He-like iron (Fe XXV) is regarded as a pure thin thermal plasma component, and its spatial distribution has been studied by Uchiyama et al. (2011). The spatial profile in the GRXE region ($|l| > 1^\circ.5$) was well fitted by a stellar mass distribution model, but the profile in the GCDX region ($0^\circ.2 < |l| < 1^\circ.5$) showed fourfold excess. Uchiyama et al. (2011) therefore concluded that the Fe XXV $K\alpha$ line in the GCDX could not be explained in the same way as the GRXE. The GRXE seems to be dominated by faint X-ray point sources such as coronally active binaries (ABs) and cataclysmic variables (CVs) (Revnivtsev et al. 2006; Revnivtsev et al. 2009; Yuasa et al. 2012). These sources belong to the old (\gtrsim Gyr) stellar population, and their X-ray luminosity function normalized to the stellar mass is not expected to vary significantly across the Galaxy (Sazonov et al. 2006).

Uchiyama et al. (2011) compared the spatial profile of the Fe XXV $K\alpha$ line with the stellar mass distribution of the nuclear bulge (NB) of the Galaxy, following Munro et al. (2006); they both

employed the elaborate stellar mass distribution model of the NB (distance from the Galactic center $R \lesssim 300\text{pc}$ or $|l| \lesssim 2^\circ$) by Philipp et al. (1999), Mezger et al. (1999), and Launhardt et al. (2002), together with additional information about the more extended part of the Galactic bulge (GB; $R \lesssim 3\text{kpc}$ or $|l| \lesssim 20^\circ$) and disk (Kent et al. 1991). The NB model is an empirical 3-D axisymmetric model consisting of a spherical nuclear stellar cluster and a nuclear stellar disk. It is mainly based on the COBE $4.9\ \mu\text{m}$ surface brightness map with an angular resolution of $0.^\circ7$. Since the NB is unresolved in Galactic latitude, the scale height of warm dust derived from IRAS data was substituted for the stellar disk. Uchiyama et al. (2011) and Munro et al. (2006) in turn integrated the NB (and GB) model along the line of sight toward the Galactic center while tuning the relative weight of each component, and compared these model surface densities with the observed surface density of the Fe XXV $K\alpha$ line. Munro et al. (2006), however, estimated the overall uncertainty in building this model to be as large as 50%.

Here we take another approach to this problem: directly comparing the observed surface density of the Fe XXV $K\alpha$ line with the observed (and extinction-corrected) stellar number density $N(l, b)$ in the K_S band, without making use of any models for the NB or GB. Since the NB and GB are highly concentrated¹ toward the Galactic center, the line of sight depth can be neglected, to 0th order. Therefore, all the stars, as well as the Fe XXV $K\alpha$ emission, can be considered to be located at a distance of 8 kpc. Then the absolute magnitude M_{K_S} and extinction-corrected apparent magnitude $K_{S,0}$ of stars are related simply by $M_{K_S} + 14.52 = K_{S,0}$, where 14.52 is the distance modulus. We aim to probe the (l, b) distribution of the old population to which the faint X-ray point sources belong, by counting stars more luminous than M_{K_S} or, equivalently, brighter than the apparent magnitude $K_{S,0}$. As a first assumption, if we set the limiting magnitude to be reasonably faint, we will be able to detect a representative old red giant population and the derived (l, b) distribution $N(K_{S,0}; l, b)$ should be similar to that of faint X-ray point sources. The earliest and faintest M giants have $M_{K_S} = -4.14$ (Wainscoat et al. 1992). We thus require a corresponding limiting magnitude of $K_{S,0} \sim 10.4$. If we cannot set the limiting magnitude faint enough, we will end up detecting only supergiants and other younger stars, whose spatial distribution can be very different. In this *Paper*, employing large-scale near-infrared survey data with faint limiting magnitudes, we derive the number density map of stars to the extinction-corrected magnitude $K_{S,0}$ deep enough to detect the old red giant population, and estimate the (l, b) distribution of faint X-ray point sources.

¹ A simple calculation based on the Wainscoat et al. (1992) model shows that only ~ 7 percent stars along the line of sight ($l = 2^\circ, b = 0$) are located at a distance of 7.5 kpc or less from the Sun.

2 Observation and Data Analysis

The central region of our Galaxy $|l| \lesssim 3^\circ.0$ and $|b| \lesssim 1^\circ.0$ (equivalent to $0.8 \text{ kpc} \times 0.3 \text{ kpc}$ for $R_0 = 8 \text{ kpc}$) was observed (Nishiyama et al. 2006) using the near-infrared camera SIRIUS (Simultaneous Infrared Imager for Unbiased Survey; Nagashima et al. 1999; Nagayama et al. 2003) on the 1.4m IRSF telescope. The SIRIUS camera provides J ($1.25 \mu\text{m}$), H ($1.63 \mu\text{m}$), and K_S ($2.14 \mu\text{m}$) images simultaneously, with a field of view of $7'.7 \times 7'.7$ and a pixel scale of $0''.45$. The typical seeing was $1''.2$ FWHM, and the averages of the $10\text{-}\sigma$ limiting magnitudes were $J = 17.1$, $H = 16.6$, and $K_S = 15.6$. We will employ only the H and K_S data because of heavy extinction toward the Galactic center.

We choose stars near the Galactic center, and derive their extinction-free magnitudes from $H - K_S$ vs K_S color magnitude diagrams (CMDs). Three by three fields of view were treated as one region of $20' \times 20'$. Figure 1 is the CMD of a region centered at $(l, b) = (-0^\circ.41, 0^\circ.53)$, shown as an example. Estimates based on a simple model (Wainscoat et al. 1992) show that the majority of detected stars are near the Galactic center and reddened to the color corresponding to $H - K_S \gtrsim 0.5$. Therefore, the stars near the Galactic center are selected by eye in the CMDs, and then their K_S magnitudes were corrected for extinction. The threshold of $H - K_S$ was 0.7 for the region shown in Figure 1, and was in the range of $0.35 - 1.10$ for each region of the whole observation. The average intrinsic color $(H - K_S)_0$ of the detected stars on the basis of calculations, considering the limiting magnitudes and using the Wainscoat et al. (1992) model, is 0.203; its standard deviation is quite small because the intrinsic color $(H - K_S)_0$ of stars is 0.0 for the bluest (rare OB stars) and 0.4 for the reddest (rare late M giants). Therefore, we regard the intrinsic color $(H - K_S)_0$ of all stars as 0.203, and corrected their K_S magnitudes according to the reddening law by Nishiyama et al. (2006) $A(K_S) = 1.44 \times [(H - K_S) - (H - K_S)_0]$; see the arrow in Figure 1. Thus we obtain the line-of-sight extinction $A(K_S)$ and extinction-corrected magnitude $K_{S,0}$ of each star.

There has been considerable work carried out on the near-IR extinction in the Galactic bulge. Some of **the work indicates** that the wavelength dependence of near-IR extinction varies **sufficiently** from one line of sight to another that the use of a single extinction law can lead to **an incorrect** stellar distribution. Nataf et al. (2013) derived I -band extinction laws as a function of two colors of $(J - K_S)$ and $(V - I)$, and concluded that the conversion from reddening to extinction cannot be done accurately with a single law. Chen et al. (2013) found large variations in extinction over angular scales as small as $15' \times 15'$. Furthermore, they found ‘grayer’ extinction coefficient A_λ/A_{K_S} toward the inner Galaxy, where λ is the Spitzer IRAC bands of 3.6 , 4.5 , 5.8 , and $8.0 \mu\text{m}$. We have checked the **impact** of such a variation, assuming that the H -band extinction coefficient changes as much as the $3.6 \mu\text{m}$ coefficient. While the *variation* in $A_{3.6}/A_{K_S}$ over the central several degrees of longitude

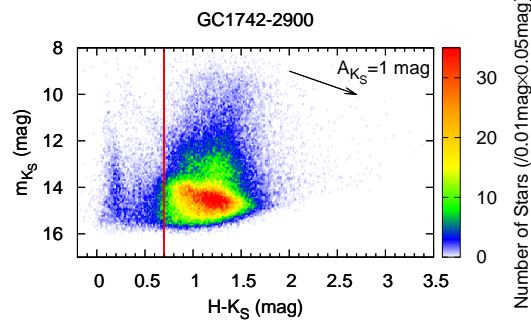


Fig. 1. The color magnitude diagram ($H - K_S$ vs K_S) of the $20' \times 20'$ region centered at $(l, b) = (-0^\circ.41, 0^\circ.53)$. Stars to the right of red line are selected as the stars near the Galactic center. These stars are dereddened oppositely to the arrow based on Nishiyama et al. (2006), to the intrinsic color of red giants $(H - K_S)_0 = 0.2$.

seems one percent at most (see their Fig.24(a)), this variation affects the dereddening procedure and leads to **a several percent change in the number count**. Thus we should be careful if we discuss more subtle differences.

We set the limiting magnitude $K_{S,0} = 10.5$, and plotted the stellar number density profile $N(10.5; l, b)$. This corresponds to the absolute magnitude of $M_{K_S} = -4.0$, which includes all M-type giants at the Galactic center. They are numerous enough (nearly two orders of magnitude more than young supergiants in the Wainscoat et al. (1992) model) to probe the old stellar population, and we therefore assume that $N(10.5; l, b)$ traces adequately the spatial distribution of faint X-ray point sources. In fact, Nishiyama et al. (2013) use a synthetic CMD computation (Aparicio & Gallart 2004) to estimate the fraction of the stars brighter than $K_{S,0} = 10.5$ **for** several different models of star forming history; they found that these bright stars trace the spatial distribution of the faint old stars very well, even in a conservative case.

Since our $10\text{-}\sigma$ limiting magnitudes are $(H, K_S) = (16.6, 15.6)$ and the extinction is $A(K_S) \sim 2 - 3.5$ mag even for the Galactic center itself (Schödel et al. 2010, the $40'' \times 40''$ region around Sgr A*), we can assume that our star list is nearly complete to the extinction-corrected magnitude $K_{S,0} = 10.5$ over almost all the regions near the Galactic center.

First, we examine this assumption. We construct an extinction-free map of the stellar number density $N(10.5; l, b)$ with a $1'$ resolution in Figure 2(a). Using these bright stars of $K_{S,0} < 10.5$, we can estimate the average extinction towards these stars at a resolution of $1'$ as well. We can check if the extinction derived in this way is consistent with the extinction $A(K_{S,\text{Spitzer}})$ derived from Spitzer/IRAC observation between 3.6 and $8.0 \mu\text{m}$ (Schultheis et al. 2009). Since the Spitzer/IRAC extinction values were derived from longer wavelength observations, they tend to represent the line-of-sight extinction

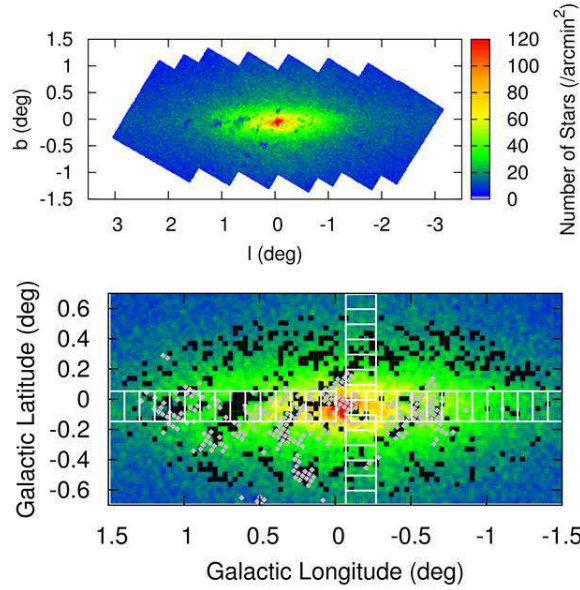


Fig. 2. (a) The number density $N(10.5; l_*, b_*)$ (arcmin^{-2}) of stars whose extinction-corrected K_S are brighter than 10.5. (b) Close-up of the central region. The same fields of view as Uchiyama et al. (2011), where the Fe xxv $K\alpha$ line intensity and $N(10.5; l_*, b_*)$ are plotted in Figure 4, are shown by *white*-outlined rectangles. Line of sight extinction derived from Spitzer/IRAC observations $A(K_{S,\text{Spitzer}})$ is greater than 3 in *gray* squares, and stellar distribution evidently decreases from the adjacent regions in *black* squares. These squares are removed from further analysis.

to the Galactic center better in more reddened regions. The comparison of these extinction values in Figure 3 indicates that our estimates agree very well with those from Spitzer/IRAC up to the extinction of $A(K_{S,\text{Spitzer}}) \sim 3$. In some of the more reddened regions, however, our extinction is smaller than Spitzer/IRAC. Therefore, we mark the map pixels whose $A(K_{S,\text{Spitzer}}) > 3$ by gray squares in Figure 2(b). Figure 2(b) has another type of squares: the black squares are the $2' \times 2'$ regions (four pixels combined) where our stellar distribution evidently decreases from the adjacent regions. To select these pixels, we have calculated the running mean of the stellar density in 15 regions of $2' \times 2'$ in l and b . These lines of sight might suffer so great an extinction that even $A(K_{S,\text{Spitzer}})$ might have been underestimated. These two types of pixels tend to increase toward the central region, and this leads to underestimation of the stellar number density in the central region. The masked pixels were removed from further analysis, which amount to 18 percent of the area of Figure 2(b).

Second, we estimate the effect of confusion on finding stars. The stellar density increases by a factor of ~ 5 from the outer part of our data to the central $0^\circ.1$. We computed the completeness of finding stars over the entire field. We added artificial sources of $K_S = 12.5$ to the SIRIUS images, and examined the recovery rate of these sources (see also Hatano et al. 2013). It is generally quite high $\sim 97\%$ in the outer part, but drops to $\sim 92\%$ in the center. Therefore, the stellar number density is slightly underestimated in the central part, and this distorts the profile slightly. We will correct for

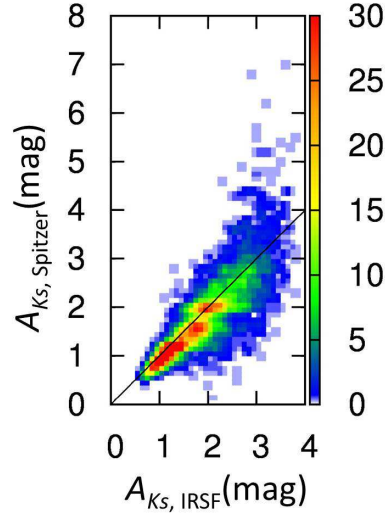


Fig. 3. The extinction derived from IRSF data (current work) and that derived from Spitzer/IRAC data (Schultheis et al. 2009). The regions whose $A(K_{S, \text{Spitzer}}) > 3$ deviate from the straight line, and are shown as gray squares in Figure 2(b).

these completeness changes in the analysis in the next section.

To check further whether the stellar number density $N(10.5; l, b)$ is not severely underestimated in the central part of our map, we constructed the number density $N(8.0; l, b)$ of stars brighter than $K_{S,0} = 8.0$ because brighter stars are less affected by confusion and extinction problems, which generally increases toward the center. We test if $N(10.5; l, b)$ and $N(8.0; l, b)$ show similar profiles. In the outer part, the two generally agree within the Poisson errors, although $N(8.0; l, b)$ is sometimes too small to make any meaningful comparison. In the central part, we calculate the averages of $N(10.5; l, b)/N(8.0; l, b)$ in the four $20' \times 20'$ regions adjacent to the central $20' \times 20'$ region. The ratio is quite constant ~ 7.3 , with a region to region variance of 0.6. In the eight $7' \times 7'$ sub-regions in the central $20' \times 20'$ region², when we multiply $N(8.0; l, b)$ by this ratio, the results are greater than $N(10.5; l, b)$ by factors 0.97 – 1.50. The mean of these factors is 1.21, i.e., greater than 1.00; this could be due to 1) the extinction or confusion mentioned above, or 2) actual change in the bright-to-faint star ratio. The latter is possible if the central part of NB contains younger stars which are often more luminous. If we were affected by this effect, then we would overestimate the point-source-originated Fe XXV $K\alpha$ emission from $N(8.0; l, b)$ in the central region. However, we would certainly be able to determine reliable upper limits. Therefore, we will use these corrected $N(10.5; l, b)$, derived from $N(8.0; l, b)$, in the central $20'$ region in the next section.

² One region of $20' \times 20'$ consists of nine $7' \times 7'$ sub-regions, but the very central sub-region is so crowded with the stars belonging to the central-parsec cluster, we did not derive the stellar density reliably. See Nishiyama et al. (2013).

3 Results and Discussion

The stellar number density distribution is compared with that of the Fe XXV $K\alpha$ line obtained with the X-ray Imaging Spectrometer onboard the Suzaku satellite reported in Uchiyama et al. (2011). We will use the new coordinates whose origin is at Sgr A*, $(l_*, b_*) = (l + 0^\circ.056, b + 0^\circ.046)$, following Uchiyama et al. (2011). The Fe XXV $K\alpha$ intensity shows several tens of percent excess on the positive l_* side (east) in comparison with the negative side (west) near the center $0^\circ.1 \leq |l_*| \leq 0^\circ.3$ (Koyama et al. 2007; Koyama et al. 2009; Uchiyama et al. 2011). This asymmetry was also pointed out in the number of X-ray stars by Munro et al. (2009). They suggest that the excess is due to young massive stars associated with the high activity of star formation in the positive l_* part. In contrast, our measurement of the near-infrared stellar number density shows no significant asymmetry, as shown in Figure 4(b). Here we compare the Fe XXV $K\alpha$ intensity and the near-infrared stellar number density on the negative l_* side where the former increases towards the center at a slower rate.

The number density $N(l_*, b_*)$ in the same rectangular bins as Uchiyama et al. (2011), $(\Delta l_*, \Delta b_*) = (0^\circ.1, 0^\circ.2)$ for the longitude distribution is plotted in Figure 4(a), and $(\Delta l_*, \Delta b_*) = (0^\circ.2, 0^\circ.1)$ for the latitude distribution, is in Figure 4(b). The center of each rectangle is given as $(l_*, b_*) = (0^\circ.1 \times n, 0.)$ along the longitude, and $(l_*, b_*) = (-0^\circ.114, 0^\circ.1 \times n)$ along the latitude, where n is a non-zero integer. The number density in each rectangular bin corresponds to the average in the unmasked $1' \times 1'$ pixels shown in Figure 2(b), and the averaged location of them is also calculated for that specified rectangle. In Figure 4(a) and (b), we normalize the stellar number density so that the ordinates agree in the GRXE region ($1^\circ.5 \leq |l_*| \leq 2^\circ.8, b_* = 0^\circ.0$), where Revnivtsev et al. (2006) found that the Fe XXV $K\alpha$ line intensity can be explained by X-ray point sources. The Fe XXV $K\alpha$ line intensity shows significant excess in comparison with the stellar number density in the central region, and the excess increases as we approach the center. The excess is ~ 1.5 at $l_* = -0^\circ.7$, and reaches ~ 2 at $l_* = -0^\circ.1$ when normalized in the Galactic ridge. The profiles in the Galactic latitude show the same tendency as shown in Figure 4(b).

$N(10.5; l_*, b_*)$ increases to the Galactic center as $|l_*|^{-0.30 \pm 0.03}$ at $b_* = 0^\circ$ in the range of $-0^\circ.1 \geq l_* \geq -0^\circ.7$, and the increase of the Fe XXV $K\alpha$ line intensity in Uchiyama et al. (2011) does as $|l_*|^{-0.44 \pm 0.02}$. The difference in these indices are independent of the region we choose for the normalization. Therefore, the Fe XXV $K\alpha$ line is likely to originate from emitters with different spatial distribution from the old population.

Our excess estimate is ~ 2 at $l_* = -0^\circ.1$, but Uchiyama et al. (2011) concluded that the emissivity in the NB must be higher by a factor of 3.8 ± 0.3 than that in the GRXE when fitted with stellar mass distribution models. If we look at their Fig. 4 (similarly the lower-right panel of Fig.

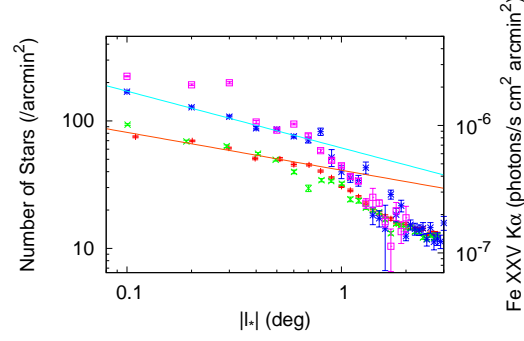


Fig. 4. (a) The stellar number density distribution $N(10.5; l_*, b_*) (\text{arcmin}^{-2})$ along the Galactic plane as a function of l_* (distance from Sgr A $_*$), *red*: negative Galactic longitude and *green*: positive. The error bars are Poisson errors, and include the uncertainty in the conversion from $N(8.0; l_*, b_*)$ for the central two positions. Also shown is Fe XXV K α line intensity distribution ($\text{photons s}^{-1} \text{cm}^{-2} \text{arcmin}^{-2}$), *blue*: negative Galactic longitude and *magenta*: positive. Note that the *blue* and *magenta* crosses are exactly at $|l_*| = 0.1, 0.2, \dots$, while the *red* and *green* crosses are slightly off because the averaged position in the rectangles in Figure 2(b) is not necessarily their centers because of the exclusion of gray and black squares in Figure 2(b). The ordinates are set so that Fe XXV K α emission and N agree in the region $-1^\circ.5 \geq l_* \geq -2^\circ.8$. Power-law approximation in the region $-0^\circ.1 \geq l_* \geq -0^\circ.7$ yields the indices of -0.44 ± 0.02 and -0.30 ± 0.03 .

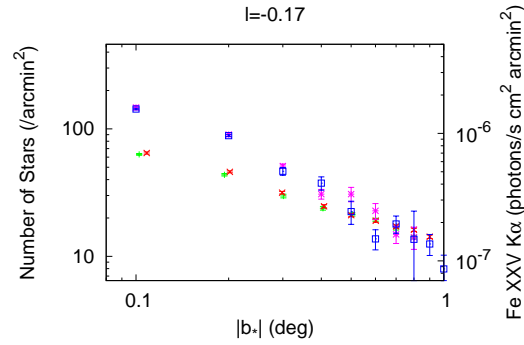


Fig. 4. (b) Same as (a), along the Galactic longitude of $l_* = -0^\circ.114$ as a function of b_* . The crosses are *magenta*: Fe XXV K α , $l_* > 0$, *blue*: Fe XXV K α , $l_* < 0$, *green*: $N(10.5)$, $l_* > 0$, *red*: $N(10.5)$, $l_* < 0$.

7 of Heard and Warwick 2013), the stellar mass distribution curve based mainly on Launhardt et al. (2002) seems to be very flat compared with the Fe XXV $K\alpha$ distribution, especially in the range of $0^\circ.1 \lesssim |l_*| \lesssim 0^\circ.7$. The stellar mass model assumes a nuclear stellar disk whose radius is about 150 pc, and the projected surface density is rather flat. In contrast, our stellar number density increases gradually toward the center. Its increase from $l = 0^\circ.7$ to $l = 0^\circ.1$ is about 1.4 times that of the flatter mass model by Launhardt et al. (2002). This difference in the stellar number density profile likely explains part of the large emissivity difference derived from our analysis and that of Uchiyama et al. (2011). Also, we have normalized the infrared/X-ray ratio in the range of $1^\circ.5 \leq |l_*| \leq 2^\circ.8$ with a slightly greater value than Uchiyama et al. (2011) because we have not included lower X-ray intensities around $l = 8^\circ$ in Fig. 4 of Uchiyama et al. (Data by Yamauchi et al. 2009). This leads to slightly smaller value in the current estimate than 3.8 in Uchiyama et al. (2011).

Another remarkable feature of Figure 4(a) is the apparent change in these slopes around $l_* = 0^\circ.8$ both in $N(10.5; l_*, b_*)$ and the Fe XXV $K\alpha$ line intensity. Within this Galactic longitude, the nuclear disk component is dominant in the stellar mass distribution model of the NB (Launhardt et al. 2002). This indicates that the Fe XXV $K\alpha$ line excess is related to the nuclear disk, and more concentrated to the center than its usual stellar component.

Finally, we discuss the possible systematic errors of the measured stellar number density. Although we corrected for the change in star-finding completeness and adopted the larger $N(10.5; l_*, b_*)$ derived from brighter stars of $K_{S,0} < 8.0$, the data point at $l_* = -0^\circ.1$ shows a slight downward shift from the straight line in Figure 4(a). To be conservative, we tried fitting without this data point, and obtained -0.36 ± 0.03 as the index of stellar number density distribution. When the point at $l_* = -0^\circ.1$ is excluded, the index of the Fe XXV $K\alpha$ distribution is -0.47 ± 0.03 . Thus even with these exclusions, the slopes seem to be different.

Thus, the diffuse X-ray emission characterized by the Fe XXV $K\alpha$ lines in the range of $|l_*| \lesssim 3^\circ.0$ and $|b_*| \lesssim 1^\circ.0$ most likely arises from 1) a point-source component which is detected as old red giants in our infrared survey and extends to the outer part of the GB, and 2) a more concentrated component which becomes prominent inside $|l_*| \leq 0^\circ.8$. The second component might be related to the NB of the Galaxy, where active star formation takes place (see, e.g., Matsunaga et al. 2011). Supernova explosions of newly born stars might be able to provide hot plasma, but the confinement of such plasma is another difficult problem, which was discussed in Nishiyama et al. (2013).

4 Summary

Direct comparison of the observed surface density of the Fe XXV $K\alpha$ line with the extinction-corrected stellar number density observed in the K_S band yields different power-law indices $|l_*|^{-0.44\pm0.02}$ and $|l_*|^{-0.30\pm0.03}$, respectively, in the range of $-0^\circ.1 \geq l_* \geq -0^\circ.7$. The Fe XXV $K\alpha$ line intensity shows significant excess in comparison with the stellar number density in the central region: ~ 1.5 at $l_* = -0^\circ.7$, and reaches ~ 2 at $l_* = -0^\circ.1$ when normalized in the Galactic ridge. Therefore, we conclude that the diffuse X-ray emission in the Galactic Center region cannot be explained solely by a population of unresolved point-sources that is related to the old stellar population.

We are grateful to the SAAO staff for their outstanding support of the operations of IRSF. We would also like to thank J. H. Hough for very helpful comments. This work was partly supported by the Grants-in-Aid Scientific Research (C) 21540240, and the Global COE Program “The Next Generation of Physics, Spun from Universality and Emergence” from the Ministry of Education, Culture, Sports, Science and Technology (MEXT) of Japan. RS acknowledges support by the Ramón y Cajal programme and by grants AYA2010-17631 and AYA2009-13036 of the Spanish Ministry of Economy and Competitiveness and by grant P08-TIC-4075 of the Junta de Andalucía. SN acknowledges support by the Grant-in-Aid for Specially Promoted Research 22000005, and Grant-in-Aid for Young Scientists (A) 25707012. We warmly thank the anonymous referee for helpful comments which improved the presentation of this paper.

References

- Aparicio, A., & Gallart, C. 2004, *AJ*, 128, 1465
- Chen, B. Q., Schultheis, M., Jiang, B. W., Gonzalez, O. A., Robin, A. C., Rejkuba, M., & Minniti, D. 2013, *A&A*, 550, A42
- Hatano, H., et al. 2013, *AJ*, 145, 105
- Heard, V. and Warwick, R. S. 2013, *MNRAS*, 428, 3462
- Kent, S. M., Dame, T. M., & Fazio, G. 1991, *ApJ*, 378, 131
- Koyama, K., Awaki, H., Kunieda, H., Takano, S., & Tawara, Y. 1989, *Nature*, 339, 603
- Koyama, K., Maeda, Y., Sonobe, T., Takeshima, T., Tanaka, Y., & Yamauchi, S. 1996, *PASJ*, 48, 249
- Koyama, K., et al. 2007, *PASJ*, 59, S245
- Koyama, K., et al. 2009, *PASJ*, 61, S255
- Launhardt, R., Zylka, R., & Mezger, P. G. 2002, *A&A*, 384, 112
- Matsunaga et al. 2011, *Nature*, 477, 188

- Mezger, P. G., Zylka, R., Philipp, S., & Launhardt, R. 1999, A&A, 348, 457
- Muno, M. P., Bauer, F. E., Bandyopadhyay, R. M., & Wang, Q. D. 2006, ApJS, 165, 173
- Muno, M. P., et al. 2009, ApJ, 181, 110
- Nagashima, C., et al. 1999 in Star Formation 1999, ed. T. Nakamoto (Nobeyama: Nobeyama Radio Obs.), 397
- Nagatomo, S., et al. in preparation
- Nagayama, T., et al. 2003 Proc. SPIE, 4841, 459
- Nishiyama, S., et al. 2006, ApJ, 647, 1093
- Nishiyama, S., et al. 2013, ApJL, 769, L28
- Nataf, D. M., et al. 2013, ApJ, 769, 88
- Philipp, S., Zylka, R., Mezger, P. G., Duschl, W. J., Herbst, T., & Tuffs, R. J. 1999, A&A, 348, 768
- Revnivtsev, M., Molkov, S., & Sazonov, S. 2006, MNRAS, 373, L11
- Revnivtsev, M., Sazonov, S., Churazov, E., et al. 2009, Nature, 458, 1142
- Sazonov S., Revnivtsev M., Gilfanov M., Churazov E., Sunyaev R. 2006, A&A, 450, 117
- Schödel, R., Najarro, F., Muzic, K., & Eckart, A. 2010, A&A, 511, A18
- Schultheis, M., Sellgren, K., Ramirez, S., Stolovy, S., Ganesh, S., Glass, I. S., & Girardi, L. 2009, A&A, 495, 157
- Uchiyama, H., Nobukawa, M., Tsuru, T. G., Koyama, K., & Matsumoto, H. 2011, PASJ, 63, 903
- Wainscoat, R. J., Cohen, M., Volk, K., Walker, H. J., & Schwartz, D. E. 1992, ApJS, 83, 111
- Yamauchi, S., et al. 2009, PASJ, 61, S225
- Yuasa T., Makishima K., & Nakazawa K. 2012, ApJ, 753, 129